BJ www.biochemj.org

BJ Signal

Biochem. J. (2011) **435**, 441–450 (Printed in Great Britain) doi:10.1042/BJ20110013

Involvement of the recoverin C-terminal segment in recognition of the target enzyme rhodopsin kinase

Evgeni Yu. ZERNII*[1], Konstantin E. KOMOLOV*†[1,2], Sergei E. PERMYAKOV‡, Tatiana KOLPAKOVA*, Daniele DELL'ORCO†, Annika POETZSCH†, Ekaterina L. KNYAZEVA‡, Ilya I. GRIGORIEV*, Eugene A. PERMYAKOV‡, Ivan I. SENIN*, Pavel P. PHILIPPOV* and Karl-Wilhelm KOCH†[2]

*A.N. Belozersky Institute of Physico-Chemical Biology, M.V. Lomonosov Moscow State University, 119991 Moscow, Russia, †Biochemistry Group, Department of Biology and Environmental Sciences, University of Oldenburg, D-26111 Oldenburg, Germany, and ‡Institute for Biological Instrumentation of the Russian Academy of Sciences, Pushchino, 142290 Moscow, Russia

NCS (neuronal Ca^{2+} sensor) proteins belong to a family of calmodulin-related EF-hand Ca^{2+}-binding proteins which, in spite of a high degree of structural similarity, are able to selectively recognize and regulate individual effector enzymes in a Ca^{2+}-dependent manner. NCS proteins vary at their C-termini, which could therefore serve as structural control elements providing specific functions such as target recognition or Ca^{2+} sensitivity. Recoverin, an NCS protein operating in vision, regulates the activity of rhodopsin kinase, GRK1, in a Ca^{2+}-dependent manner. In the present study, we investigated a series of recoverin forms that were mutated at the C-terminus. Using pull-down assays, surface plasmon resonance spectroscopy and rhodopsin phosphorylation assays, we demonstrated that truncation of recoverin at the C-terminus significantly reduced the affinity of recoverin for rhodopsin kinase. Site-directed mutagenesis of single amino acids in combination with structural analysis and computational modelling of the recoverin–kinase complex provided insight into the protein–protein interface between the kinase and the C-terminus of recoverin. Based on these results we suggest that Phe^{3} from the N-terminal helix of rhodopsin kinase and Lys^{192} from the C-terminal segment of recoverin form a cation–π interaction pair which is essential for target recognition by recoverin. Taken together, the results of the present study reveal a novel rhodopsin-kinase-binding site within the C-terminal region of recoverin, and highlights its significance for target recognition and regulation.

Key words: calcium-feedback mechanism, cation–π interaction, neuronal calcium sensor (NCS) protein, rhodopsin kinase (RK), ternary protein complex, visual phototransduction.

INTRODUCTION

Various aspects of neuronal function are regulated by changes in intracellular Ca^{2+} concentration. The intensity and duration of Ca^{2+} signals can trigger the activation of different Ca^{2+} pathways leading to specific physiological effects [1]. Eventually the large diversity of Ca^{2+}-regulated events is the result of the action of Ca^{2+}-sensor proteins, which transform Ca^{2+} signals into a wide range of cellular responses. The specificity of such transduction pathways depends on the affinity of the Ca^{2+} sensor for Ca^{2+}, on the intracellular localization of the Ca^{2+} sensor and on the ability of the Ca^{2+} sensor to interact with effector enzymes [2]. Ca^{2+}-sensor proteins contain specific structural elements, such as EF-hand motifs or C2-domains that recognize and bind Ca^{2+} in a highly sensitive and specific manner [3,4]. Binding of Ca^{2+} triggers conformational changes in the protein, enabling the protein to specifically modulate the activity of intracellular effector proteins [several Ca^{2+} sensors can modulate the activity of the target proteins in Ca^{2+}-free (apo-) form] [5].

Although some of the known Ca^{2+} sensors are ubiquitous, the expression of others is restricted to certain tissues or cell types. The most common ubiquitous Ca^{2+} sensor is calmodulin which is widely expressed and regulates a large variety of targets. NCS (neuronal Ca^{2+} sensor) proteins have a more restricted expression pattern and repertoire of target proteins. This protein family can be divided into five groups based on structural and functional similarities: recoverins, visinin-like proteins, frequenins, GCAPs (guanylate cyclase-activating proteins) and KChiPs (K^{+}-channel-interacting proteins). NCS proteins are highly homologous and the three-dimensional structures of some prototypical NCS proteins show that they consist of two domains with two EF-hand-type Ca^{2+}-binding motifs each [5–7].

A distinctive feature of NCS proteins is that, in spite of a high degree of homology and structural similarity, each Ca^{2+} sensor can selectively regulate an intracellular target by sensing a specific narrow range of Ca^{2+} [5–7]. A fundamental question with respect to these observations is which structural elements account for the unique Ca^{2+}-sensitive target recognition events. Visual inspection of the primary structural alignment of NCS proteins reveals hypervariable amino acid sequence segments in the C-terminus of NCS proteins that are located after the fourth EF-hand.

Recoverin is a small NCS protein that is involved in Ca^{2+}-dependent feedback mechanisms of photoreceptor cells by regulating RK (rhodopsin kinase) activity. RK and recoverin form a ternary complex with rhodopsin, thereby preventing rhodopsin phosphorylation [8,9]. A first structural analysis of the binary RK–recoverin complex has revealed that the N-terminus

Abbreviations used: DTT, dithiothreitol; GCAP, guanylate cyclase-activating protein; GST, glutathione transferase; KChiP, K^{+}-channel-interacting protein; NCS, neuronal Ca^{2+} sensor; RK, rhodopsin kinase; RMSD, root mean square deviation; ROS, rod outer segment; SPR, surface plasmon resonance; WT, wild-type.

[1] These authors contributed equally to this work.

[2] Correspondence may be addressed to either of these authors (email konstantin.komolov@uni-oldenburg.de or karl.w.koch@uni-oldenburg.de).

of RK forms an amphipathic α-helix, which interacts with a hydrophobic groove on the exposed surface of recoverin [9,10]. The C-terminal region of recoverin (residues 190–202) was not resolved in this complex and therefore was out of scope of the intermolecular contacts revealed in this study described above . In previous biochemical and X-ray crystallographic studies we have already demonstrated that the C-terminal segment in recoverin is an internal modulator of Ca^{2+} sensitivity controlling the Ca^{2+}-myristoyl switch mechanism of recoverin and therefore the Ca^{2+}-dependence of recoverin binding to membranes and the range of Ca^{2+} concentrations for recoverin regulation of RK activity [11]. Investigation of the involvement of the recoverin C-terminus in direct binding to RK has not so far been undertaken.

In the present study we address the question of whether the C-terminus of recoverin could directly participate in the interaction with RK and, if so, what is the functional impact of this interaction on the physiological role of recoverin as an inhibitor of RK.

EXPERIMENTAL

Materials

$^{45}CaCl_2$ was purchased from PerkinElmer and [γ-^{32}P]ATP was from Hartmann Analytic. CM5 BIAcore sensor chips, BIAcore coupling reagents, GST (glutathione transferase), goat anti-GST antibody and CNBr-activated Sepharose were from GE Healthcare. All other reagents were obtained from Sigma, Merck, Fluka and Serva, and were at least analytical grade.

Cloning, heterologous expression and purification of recoverin forms

The truncated mutants of recoverin denoted $Rc^{2–196}$, $Rc^{2–192}$, $Rc^{2–190}$, $Rc^{2–188}$, $Rc^{2–187}$, $Rc^{2–186}$ and $Rc^{2–184}$, and point mutants denoted Rc^{P190G}, Rc^{Q191A}, Rc^{K192A} and Rc^{V193G} were obtained from a full-length recoverin cDNA in a pET-11d plasmid using standard site-directed mutagenesis procedures. For the production of each mutant DNA, a pair of oligonucleotide primers was employed in PCR. Primers containing the bacteriophage T7 promotor sequence were used in the forward direction and a primer containing a stop codon and BamHI restriction site instead of the codon of the target amino acid was used in the reverse direction. The PCR fragments were inserted in a pET-11d plasmid between the NcoI and BamHI restriction sites. The screening for the mutant clones was performed using BglII restriction analysis. The integrity of the insert was confirmed by sequencing using the Sanger method. Heterologous expression of myristoylated recoverin forms in *Escherichia coli* BL-21(DE3) cells and their purification from cell lysates were performed as described previously [12]. The degree of myristoylation was determined by analytical HPLC using a reversed-phase column (Phenomenex Luna 5 μ C_{18}, 4.6 mm $\times$ 250 mm) and was in most cases more than 95 %. Concentrations of purified recoverin were determined using $\varepsilon_{280} = 27500\ M^{-1}\cdot cm^{-1}$ [13].

RK constructs and native RK

The N-terminal domain of RK corresponded to amino acids Met^{1}–Gly^{183}, contained a GST-fusion part at the N-terminus and was denoted N-RK. Cloning, heterologous expression and purification of this construct was performed according to a previously published procedure [8]. The single point mutant N-RK^{F3A} was created by standard cloning techniques. Native RK was purified from bovine ROS (rod outer segment) preparations as described previously [14].

Fluorescence measurements

To determine the thermal stability of recoverin mutants, tryptophan fluorescence spectra at different temperatures were recorded using a Cary Eclipse spectrofluorimeter (Varian), equipped with a Peltier-controlled cell holder. Samples were measured in 20 mM Tris/HCl buffer (pH 8.0) containing 100 mM NaCl, 1 mM DTT (dithiothreitol) and either 1 mM $CaCl_2$ or 1 mM EDTA; the protein concentration in samples was 10–15 μM. Recording of spectra and evaluation of data was as described previously [11,15].

$^{45}Ca^{2+}$-binding assay and equilibrium centrifugation assay

Binding of $^{45}Ca^{2+}$ to WT (wild-type) recoverin and mutants, and binding of recoverin mutants to ROS membranes using an equilibrium centrifugation assay was investigated as described previously [12,16].

Phenyl-Sepharose-binding assay

The phenyl-Sepharose-binding assay was performed according to a previously published procedure [17]. Briefly, 2 μM WT recoverin or mutants were mixed with 100 μl of phenyl-Sepharose (GE Healthcare) and incubated at 37 °C (Eppendorf thermomixer, 1000 rev./min) for 15 min in 20 mM Hepes (pH 7.5), 150 mM NaCl, 20 mM $MgCl_2$, 1 mM DTT and 3 mM EGTA or 2 mM $CaCl_2$ (total volume of 1000 μl). The mixture was centrifuged for 15 min (14000 ***g***, table-top centrifuge Eppendorf model 5415), and the protein concentration in the supernatant was determined using a Bradford protein assay (Bio-Rad Laboratories).

Pull-down assay

Interaction of recoverin forms with N-RK was tested using analytical affinity chromatography (pull-down assay). A 10 μg amount (in 50 μl) of the N-RK fragment carrying a GST tag was immobilized on glutathione–Sepharose by incubating it for 1 h at 4 °C (Eppendorf thermomixer, 1200 rev./min) with 30 μl of a 75 % (v/v) suspension of glutathione–Sepharose in 20 mM Tris/HCl buffer (pH 7.5). The N-RK coupled to Sepharose was washed twice with 1 ml of a buffer containing 20 mM Tris/HCl (pH 7.5), 100 mM NaCl, 1 mM DTT, 0.05 % Tween 20 and 2 mM $CaCl_2$ or 5 mM EGTA to remove any non-bound protein. The last supernatant was removed and 10 μg of the corresponding recoverin form was applied to washed beads. The suspension was incubated for 1 h at 4 °C in the above-mentioned buffer in a total volume of 80 μl. After washing three times with 1 ml of the same buffer, the beads were treated with 30 μl of SDS sample buffer and eluted proteins were analysed by Western blotting using an anti-recoverin antibody [18].

SPR (surface plasmon resonance)

SPR measurements were performed on a BIAcore 2000 (GE Healthcare). Application of SPR technology in our laboratory and the analysis of data have been described in detail previously [19–21]. Specific adjustments of the procedure for the analysis of N-RK constructs are published in a recent paper [8].

RK assay

The assay mixture in a final volume of 50 μl contained 10 μM rhodopsin (urea-washed ROS), 20 mM Tris/HCl (pH 7.5), 3 mM $MgCl_2$,1 mM [γ-^{32}P]ATP (30–100 d.p.m./pmol), 1 mM EGTA, 1.26 mM $CaCl_2$, 1 mM DTT, 1 mM PMSF, 0.3 unit of RK and different concentrations of recoverin forms. The reaction was initiated by the addition of ATP, and samples were incubated in continuous light for 30 min at 37 °C. Incubation was terminated by adding 1 ml of 10 % (w/v) trichloroacetic acid. The resulting precipitate was collected by centrifugation and washed three or four times with 1 ml of 10 % (w/v) trichloroacetic acid; the pellet was used for Cerenkov counting.

Modelling the N-RK$^{1–25}$–recoverin complex and docking simulations

The crystallographic structure available at the highest resolution [1.50 Å (1 Å = 0.1 nm)] of non-myristoylated WT bovine recoverin (PDB entry 1OMR) was used as a template for the recoverin C-terminus [14]. The region corresponding to the amino acid stretch Glu^{181}–Gln^{187} was superimposed on the average NMR structure of the N-RK$^{1–25}$–recoverin complex [9] (PDB entry: 2I94; in such a complex only residues 1–16 of the N-RK peptide were resolved; recoverin residues 190–201 are missing), in which duplicate atoms, water molecules and hydrogens were removed. The superposition led to a Cα-RMSD (root mean square deviation) of 2.4 Å. The 2I94 complex structure was truncated at Ile^{186}, and the strand corresponding to the recoverin C-terminus (Gln^{187}–Leu^{202}) was merged from the superimposed 1OMR structure. Polar hydrogens were then added and the complex was energy-minimized in vacuum by 1500 steps of steepest descent with an average gradient tolerance of 0.001 kcal/mol (1 kcal ≈ 4.184 kJ). This procedure led to the Rc$^{8–202}$–N-RK$^{1–16}$ complex used as native in further computations (shown in Figures 4A and 7).

Truncated forms of native recoverin were prepared *in silico* (Table 1) in line with experimental variants, and three sets of rigid-body docking simulations between each recoverin variant (target) and the N-RK$^{1–16}$ peptide (probe) with randomized initial positions were performed by using a well-established protocol [22,23], thus generating for each docked complex 12 000 different solutions, i.e. corresponding to relative target/probe co-ordinates. Each *i*-docking solution is characterized by a score index (ZD*i*) that quantifies shape complementarity, electrostatics and desolvation of the interface upon binding of each docked complex [24], and is ranked accordingly (i.e. 1 = best scored solution; 12 000 = worst scored solution). For each docking simulation, the native-like solutions ZDi^N, which structurally resemble that of the native modelled complex (Cα-RMSD < 1 Å), were then clustered and analysed as described previously [25] and an average docking score (ZD-s) was calculated for each cluster starting from the score of each individual native-like complex (Table 1) (eqn 1):

$$\mathrm{ZD}-s=\frac{\sum_i \mathrm{ZD}_i^N}{M} \quad (1)$$

in which the cluster groups *M* native-like solutions. Such a ZD-s index is a convenient empirical descriptor of the affinity in protein–protein interactions occurring without major structural rearrangements as it is linearly correlated with ΔG [22]. Therefore we employed this to predict the effect of recoverin truncations on its affinity for the N-RK peptide.

Table 1 Docking simulations of the interaction of recoverin truncated forms and the RK peptide

Recoverin form*	Number of native-like solutions†	Ranking of native-like solutions‡	ZD-s§
8–202 (WT)	648 (5.4 %)	1; 1; 1	37.68 ± 0.23
8–196	594 (5.0 %)	1; 1; 1	37.25 ± 0.23
8–192	596 (5.0 %)	1; 1; 1	35.92 ± 0.19
8–190	617 (5.1 %)	3; 7; 3	34.71 ± 0.14
8–188	406 (3.4 %)	44; 64; 94	33.67 ± 0.14

*Recoverin forms used in the simulations, each form starts from residue 8, because the first seven residues were not resolved in the experimental structure (see the Experimental section).

†The number of native-like solutions, i.e. with Cα-RMSD < 1 Å with respect to the native complex are reported, out of the 12000 solutions retained for each recoverin form from three docking runs. In parentheses is the percentage of native over total solutions.

‡The rank of native like-solutions found in each of the three independent docking runs is reported.

§Average docking score of each cluster of native-like solution ± S.E.M.

RESULTS

NCS proteins exhibit high amino acid homology in the core part of their structure that mainly encompasses the EF-hand domains. A general feature of the NCS proteins structure is a number of conservative hydrophobic residues (Figure 1A, highlighted in bold) localized in the N-terminal lobe and implicated in target binding [26–28]. Differences in the amino acid sequences of NCS proteins are most prominent at the N- and C-terminal parts (Figure 1A). Based on our previous findings that the C-terminus of recoverin operates as an internal modulator of Ca^{2+} sensitivity and contributes significantly to the thermal stability of the protein [11], we set out to determine the critical amino acids and amino acid length of the C-terminus with respect to these properties. Using this approach we also found that the C-terminus participates in the interaction with RK.

We prepared several mutants of recoverin with different lengths of the C-terminal region (Figure 1B, top panel). The amino acid sequence of the shortest form Rc$^{2–184}$ ended after the fourth EF-hand of the protein. Truncated recoverin forms were purified from *E. coli* extracts after heterologous expression using a standard protocol to apparent homogeneity. They showed a decreased electrophoretic mobility consistent with their reduced molecular mass (Figure 1B, bottom panel). All recoverin forms were expressed with an attached myristoyl group as described previously for WT recoverin and other mutants. The extent of myristoylation of every recoverin mutant used in the present study was determined by reversed-phase HPLC yielding a degree of myristoylation exceeding 95 % for the mutants Rc$^{2–196}$, Rc$^{2–192}$, Rc$^{2–190}$ and Rc$^{2–188}$, whereas shorter constructs had a reduced level of myristoylation (60–80 %) indicating an altered conformation.

Thermal stability of recoverin mutants

Thermal unfolding of recoverin can be monitored by heat-induced changes in the maximum position of the fluorescence spectrum of its tryptophanyls (Figure 2). In general, the Ca^{2+}-free (apo) recoverin was less thermostable than the Ca^{2+}-bound form by 12–16 °C (Table 2). Down to a length of 188 amino acids, the truncation did not affect the thermal stability, remaining nearly constant without regard to Ca^{2+} content (Figure 2C). Further shortening of the C-terminus, however, led to decreased thermal stability. For example, apo-Rc$^{2–186}$ exhibited a decrease in mid-transition temperature for 7–9 °C (Figure 2B and Table 2). The notable decrease in thermal stability and myristoylation level

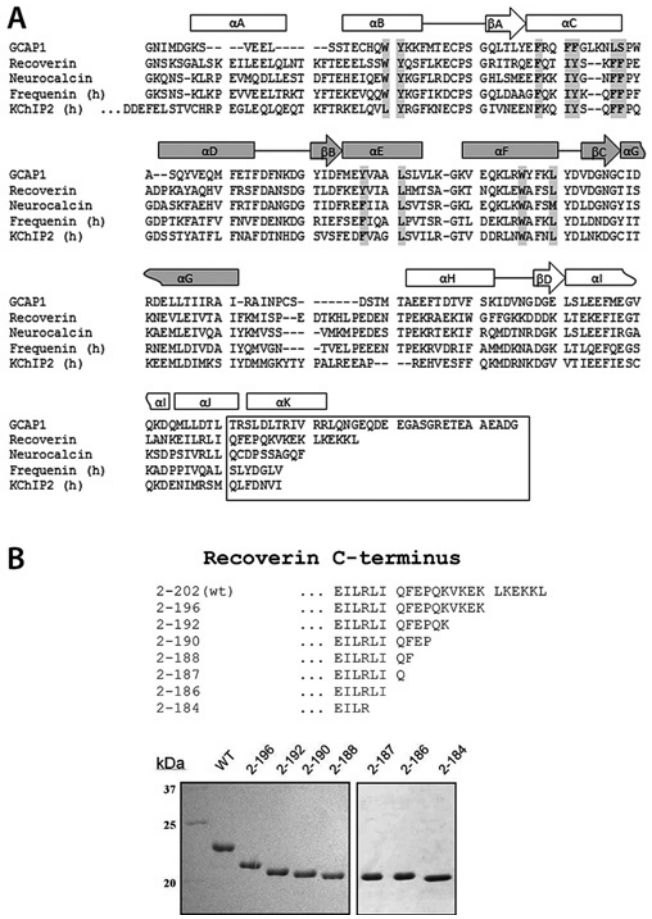

Figure 1 Comparison of NCS proteins and design of truncated recoverin forms

(**A**) Multiple sequence alignment of NCS proteins. The sequences of bovine GCAP1, recoverin and neurocalcin, and from human frequenin and KChIP1 are shown. Secondary structural elements (α-helices and β-sheets) are indicated and the functional Ca^{2+}-binding regions EF-hand 2 and EF-hand 3 are highlighted in grey. Amino acids of the hydrophobic pocket are shown in bold and framed in grey. The residues outlined in the box correspond to the 'C-terminal segment'. (**B**) SDS/PAGE analysis of purified C-terminal truncated forms of recoverin. C-terminal sequences of mutant forms in comparison with WT are shown above the gel. The molecular mass in kDa is indicated on the left-hand side.

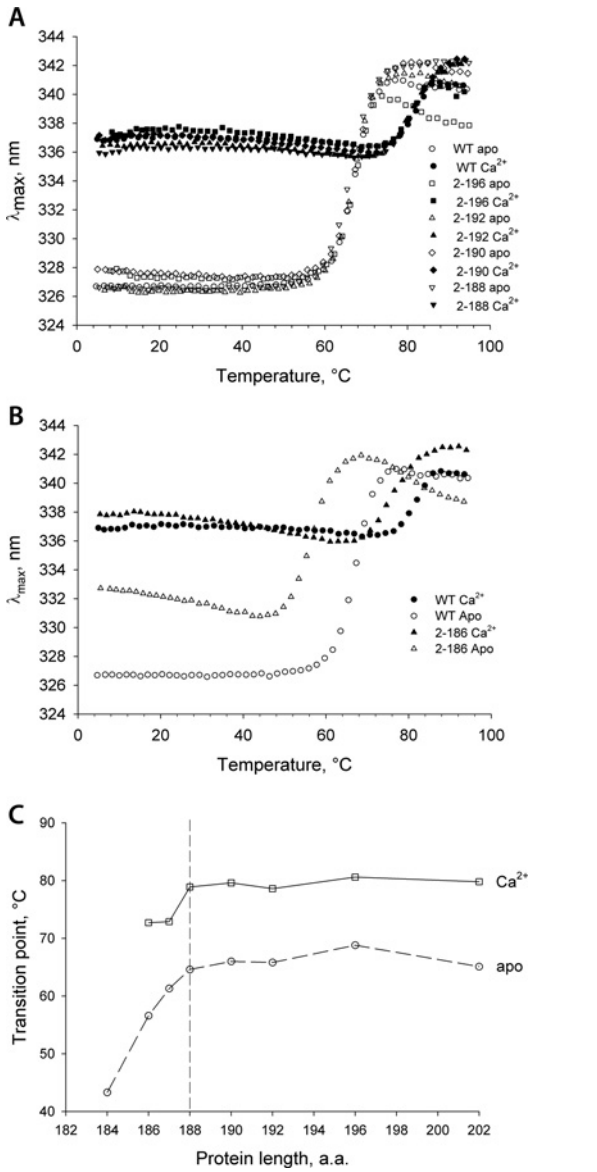

Figure 2 Thermal stability of C-terminal-truncated recoverin forms according to the data of tryptophan fluorescence of the protein

The maximum position of the fluorescence spectrum (λ_{max}) was recorded at increasing temperature in the presence of 1 mM $CaCl_2$ (closed symbols) or 1 mM EDTA (open symbols). (**A**) Thermal unfolding of truncated recoverin forms (Rc^{2-196} to Rc^{2-188}) that exhibited WT-like thermal stability. (**B**) Thermal unfolding of Rc^{2-186}, exhibiting decreased thermal stability. A similar behaviour was observed for mutants Rc^{2-187} and Rc^{2-184} (results not shown). (**C**) Mid-transition temperatures ($T_{1/2}$) for thermal unfolding of Ca^{2+}-loaded (squares) and apo-forms (circles) of truncated recoverin mutants. The $T_{1/2}$ values are plotted against protein length of recoverin. The mutants with destabilized structure are separated from the mutants with WT-like stability by a vertical broken line.

of recoverin mutants below a protein length of 188 amino acids demonstrate essential structural disturbance in the protein. Therefore the respective recoverin mutants were excluded from the further analysis.

$^{45}Ca^{2+}$ and ROS membrane binding

A step-wise truncation of the C-terminus can impair the affinity of recoverin for Ca^{2+}. Direct binding of Ca^{2+} was measured using the $^{45}Ca^{2+}$-binding assay and yielded the higher K_d values the more amino acids were cut (Table 2). Whereas Rc^{2-196} was similar to the WT, Rc^{2-188} exhibited a 2-fold lower affinity. Similarly to WT recoverin, the binding of Ca^{2+} to these mutants was co-operative as indicated by Hill coefficients between 1.55 and 1.9. The change in the affinity for Ca^{2+} in truncated recoverin mutants suggested alterations in the Ca^{2+}–myristoyl switch mechanism of the protein underlying its binding to membranes. One may expect a shift in Ca^{2+}-dependence of the binding to a higher free Ca^{2+} concentration. Indeed, as revealed from analysis of the binding of truncated recoverin forms to native washed ROS membranes, the value of half-maximal free Ca^{2+} concentration for binding to membranes of Rc^{2-196} was similar to that of WT, whereas Rc^{2-188} exhibited a 1.5-fold shift to higher free Ca^{2+} concentration (Table 2). Taken together these results showed that the C-terminus is important for regulating the Ca^{2+} sensitivity of recoverin, thereby confirming previous conclusions on the mutant Rc^{2-190} [11]. Importantly, the changes in Ca^{2+} sensitivity were not related to any mutation-induced protein-stability changes, which are absent in our case (Figure 2 and Table 2).

Table 2 The effect of recoverin C-terminal truncation on the thermal stability of the protein, its Ca^{2+}-binding parameters, Ca^{2+}-dependent interaction with ROS membranes and the affinity for N-RK

$T_{1/2}$, mid-transition temperature.

Recoverin form	Thermal denaturation*		Binding of Ca^{2+}‡		Binding to membranes§		Affinity for N-RK‖
	$T_{1/2}$ (°C): apo form	$T_{1/2}$ (°C): Ca^{2+}-bound form	K_d (μM)	Hill coefficient	EC_{50}, $[Ca^{2+}]_f$ (μM)	Hill coefficient	K_d (μM)
WT	65.1	79.8	19.2 ± 0.4	1.78	3.5 ± 0.2	2.0	10 ± 0.6
2–196	68.8	80.6	19.7 ± 0.6	1.73	3.3 ± 0.2	2.2	34 ± 1.7
2–192	65.8	78.6	26.2 ± 1.0	1.90	4.1 ± 0.3	1.75	41 ± 2.4
2–190	66	79.6	36.8 ± 3.5	1.55	5.9 ± 0.6	1.27	68 ± 3.8
2–188	64.6	78.9	41.9 ± 3.0	1.63	5.3 ± 0.5	0.9	78 ± 7
2–187†	61.3	72.9					
2–186†	56.6	72.7					
2–184†	43.3	–					

*Thermal denaturation of recoverin forms was monitored by tryptophan fluorescence of the protein.

†Recoverin forms with disturbed structural stability were excluded from further testing.

‡Ca^{2+}-binding parameters were measured by $^{45}Ca^{2+}$-binding assay.

§Binding of recoverin forms to ROS membranes was measured at different $[Ca^{2+}]_f$ using an equilibrium centrifugation assay.

‖The affinity of recoverin forms to N-RK were studied using SPR spectroscopy. The binding sensorgrams were recorded upon consecutive injections of Ca^{2+}-loaded recoverin forms at increasing concentrations over a sensorchip surface coated with N-RK via an anti-GST antibody. The equilibrium binding constants (K_d) are based on half-maximal concentration of recoverin required for saturation (Figure 3C).

Interaction with RK

The N-terminal part of RK forms an amphipathic helix that interacts with an exposed hydrophobic groove in recoverin [9,10]. We tested the interaction of truncated recoverin mutants with the N-terminal domain of RK using a pull-down assay and SPR spectroscopy (Figure 3). GST-fusion constructs of the N-terminal domain of RK (N-RK) were immobilized on glutathione–Sepharose and incubated with recoverin WT and mutants in the presence and absence of Ca^{2+}. The Ca^{2+} concentration was saturating in all cases. All recoverin forms showed a Ca^{2+}-induced interaction with N-RK, but mutants with a truncated C-terminus bound less strongly to N-RK, especially Rc^{2-190} and Rc^{2-188} (Figure 3A). We confirmed this result by immobilizing N-RK on a sensorchip surface and flushing 14 μM recoverin WT and mutants over the N-RK-coated surface. Positive amplitudes indicated binding of recoverin to N-RK and gave a first hint with regard to relative binding affinities. Mutants showed lower binding amplitudes than did WT (Figure 3B), which is in agreement with the decreased intensity of the protein bands shown in Figure 3(A). For further quantifying these results, we performed titration series with all recoverin mutants on N-RK-coated sensorchips. Recoverin forms were injected into the flow system at concentrations between 0.1 and 220 μM (Figure 3C). Apparent affinity constants (K_d in Table 2) correspond to the concentration at which the response amplitudes were half-maximal. The difference in the apparent K_d values for WT and Rc^{2-188} was 7.8-fold; the mutants Rc^{2-196}, Rc^{2-192} and Rc^{2-190} differed by factors of 3.4, 4.1 and 6.8 respectively (Table 2). We next asked whether the decrease in binding affinity might have a functional consequence in regulating RK activity. At saturating Ca^{2+} concentrations, WT recoverin prevented RK from phosphorylating rhodopsin by forming a ternary complex. Kinase activity was less inhibited by truncated mutants (Figure 3D). For example, the inhibitory response curve with Rc^{2-188} was shifted to higher concentrations of recoverin. A comparison of all tested mutants at a fixed recoverin concentration (14 μM) revealed an almost gradual decrease in inhibitory efficiency, when the C-terminus was more and more reduced (Figure 3D, inset). The shift in the inhibitory response curve is consistent with a lower affinity of the mutants for RK (Figures 3C and 3D). The lower affinity, however, did not result from a changed or disturbed exposition of hydrophobic regions in recoverin, since the mutants showed the same Ca^{2+}-dependent binding to phenyl-Sepharose as WT recoverin (results not shown). In summary, we conclude from our results that the C-terminus of recoverin not only participates in regulating its Ca^{2+} sensitivity, but also is involved in direct interaction with RK and thereby controls the inhibitory effect of recoverin.

Modelling of the recoverin–N-RK protein complex structure

To investigate whether an involvement of the C-terminus of recoverin in the interaction with the N-terminal region of RK is feasible from a structural point of view, we built a model of the recoverin–N-RK complex focusing on the interaction interface involving the C-terminus of recoverin. The available three-dimensional NMR structure of recoverin in complex with the N-terminal fragment of rhodopsin kinase ($N\text{-}RK^{1-25}$) was used as a template [9]. Furthermore, the missing C-terminal fragment of the recoverin NMR structure was taken from the crystallographic structure of non-myristoylated recoverin having this element resolved [14]. The model obtained of the complex revealed a position of the C-terminal α-helix of recoverin (highlighted in red, Figure 4A) in close proximity with the N-terminal kinase peptide (highlighted in blue, Figure 4A). Although the main part of the N-RK peptide is deeply buried inside a hydrophobic groove of recoverin, the first amino acids of the N-RK helix form a contact interface with the C-terminal region of recoverin (Figure 4A).

The resulting model was used to perform rigid-body docking simulations of the interaction process of N-RK with the truncated recoverin forms that we employed in pull-down and SPR experiments. Applied docking simulations suggested significantly different roles for the various portions of the C-terminus of recoverin in modulating RK recognition. Although the relative population of native-like solutions was the highest for WT recoverin (5.4 %; see Table 1), it remained constant to ~5.0 % for all of the subsequent truncations up to the shortest stretch (Rc^{8-188}), for which it reduced to 3.4 %. The best-scored solutions, in line, were found to be native-like in each independent docking run up to the Rc^{8-190} form, and they were ranked even lower for

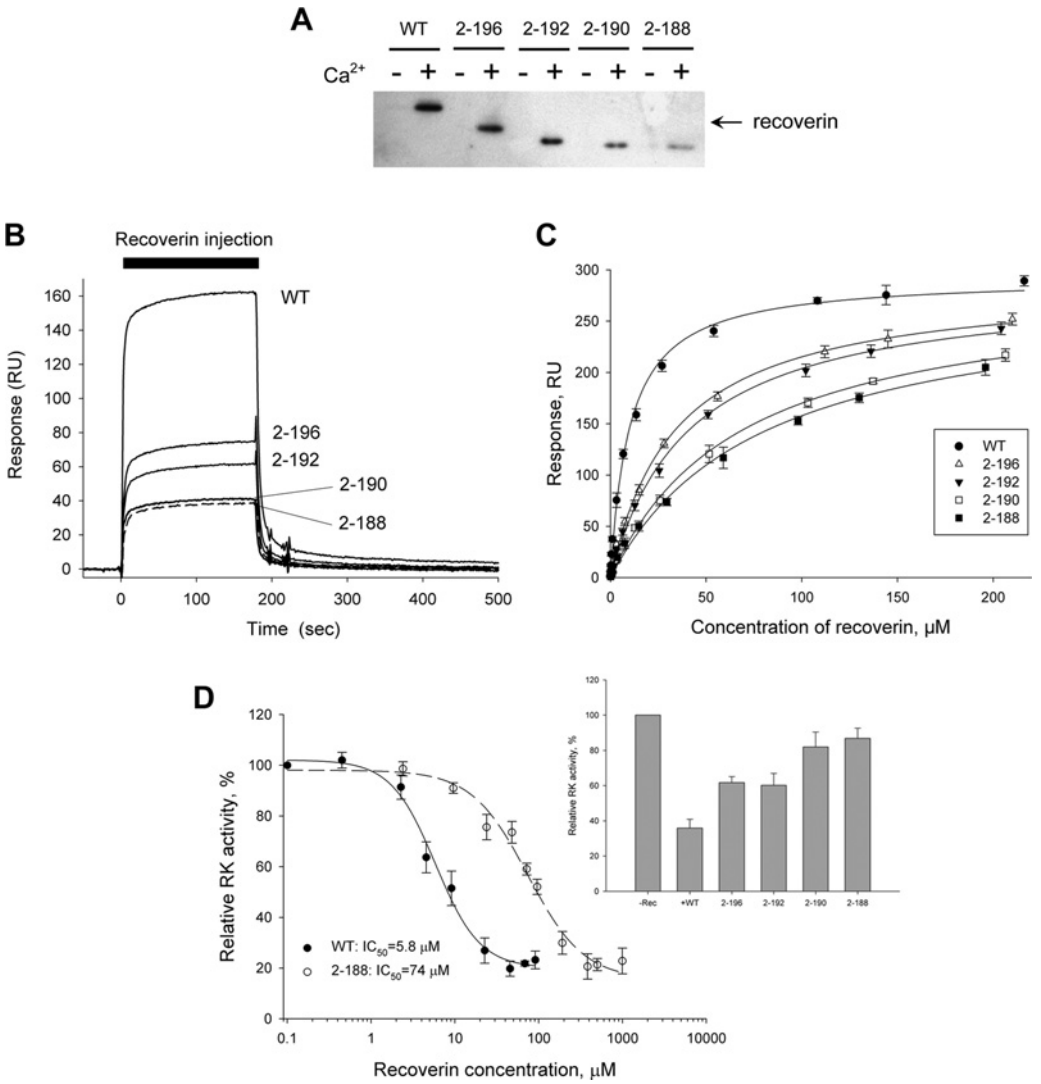

Figure 3 Effect of recoverin C-terminal truncations on its binding to N-RK

(**A**) Pull-down assay demonstrating the dependence of recoverin binding to N-RK on the length of the recoverin C-terminus. All recoverin forms containing a truncated C-terminus showed a lower binding to N-RK than WT. The N-terminal domain of RK was immobilized on glutathione–Sepharose and used to pellet apo or Ca^{2+}-loaded forms of recoverin. Bound proteins were eluted from the sorbent by SDS/PAGE sample buffer and analysed by SDS/PAGE and Western blotting. The recoverin content in each case was detected using anti-recoverin antibodies. (**B**) A representative overlay of SPR sensorgrams showing real-time binding of C-terminal-truncated recoverin mutants to N-RK. N-RK was anchored on the sensorchip surface via its GST tag using anti-GST antibodies covalently coupled to the dextran matrix. Ca^{2+}-loaded forms of recoverin were injected over the N-RK surface to obtain binding curves. The concentration of recoverin during runs in each case was 14 μM. The reference signal from a control surface with immobilized GST was subtracted. (**C**) Steady-state affinity analysis of C-terminal-truncated recoverin binding to N-RK by SPR spectroscopy. Binding of truncated recoverin forms was recorded at different concentrations of recoverin and the amplitudes of binding signals at equilibrium were determined, normalized and shown as a function of recoverin concentration. The concentration of recoverin was varied from 0.1 to 220 μM. (**D**) Inhibition of RK by WT and Rc^{2-188}. RK activity was measured by an *in vitro* phosphorylation assay in the presence of 200 μM free Ca^{2+}. The concentration of WT and mutant Rc^{2-188} was varied within 0–0.1 mM and 0–1.0 mM respectively. Phosphorylation of rhodopsin in the presence of other truncated forms of recoverin is shown in the inset and was measured at 14 μM recoverin.

the Rc^{8-188} variant. Both the statistics and the average scores of the ensembles of reconstituted complexes (Table 1) are significantly affected by the truncation, especially for the 8–190 and 8–188 variants, hence suggesting a major role for the 189–192 residues.

A highly significant correlation ($R = 0.97$) was found between the average scores of ensembles of reconstituted complexes (ZD-s) and the experimental affinity measured by SPR (Figure 4B; for clarity we have plotted the K_d instead of the $\ln K_d$ on the *x*-axis). The ZD-s index is known to linearly correlate with the free energy of binding of protein–protein complexes that form in water-soluble and in membrane environments without major conformational changes in either protein [22,23,25,29,30]. Hence such correlation corroborates the reliability of the three-dimensional model of the complex and suggests that the effect of truncation is not to perturb the remaining structure of recoverin, which appears to be stable independent of the truncated portion, a hypothesis indirectly confirmed by our thermal denaturation studies. Moreover, such correlation further suggests that the binding with the N-RK peptide may occur in a rigid-body-like manner.

Protein–protein interface of the recoverin–N-RK complex

The structural analysis of the model suggested that a stretch of residues included in the 190–193 sequence of the recoverin

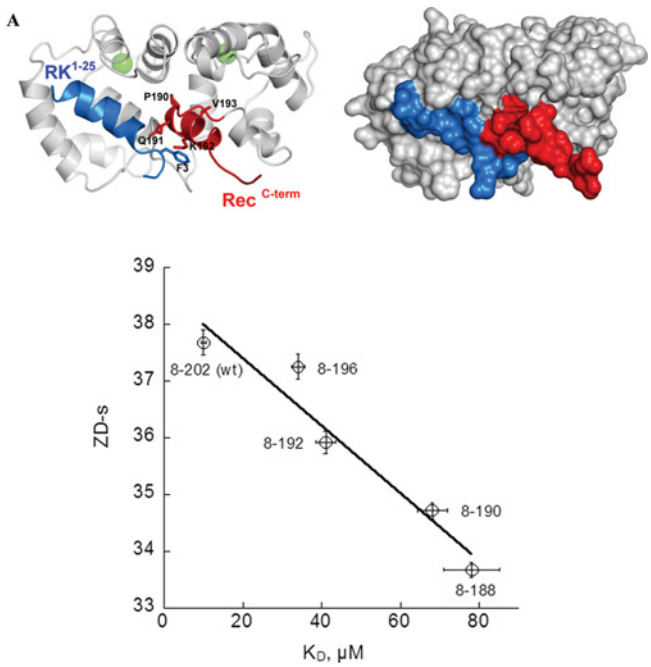

Figure 4 Modelling the recoverin–RK$^{1–25}$ complex using rigid-body docking

(**A**) Three-dimensional model of the recoverin–RK$^{1–25}$ complex. The model is based on the available NMR structure of the recoverin–RK$^{1–25}$ complex (PDB entry 2I94 [9]) fused with the X-ray crystallographic structure of the C-terminus of recoverin (PDB entry 1OMR [14]. Only residues 1–16 in RK are shown, whereas the structure of recoverin comprehends residues 8–202 (see the Experimental section). The RK$^{1–25}$ peptide is shown in blue, whereas recoverin is shown in grey, except for its C-terminus that is shown in red. Ca^{2+} are represented by green spheres. On the left-hand side, a ribbon representation shows the secondary structure of the complex, and the residues targeted by mutagenesis are labelled and shown in stick representation. On the right-hand side, the molecular surface of the complex is shown from the same perspective. (**B**) Plot of average docking scores (ZD-s) of the clusters containing native-like solutions for each truncated recoverin form against experimental affinity data for the RK peptide. The linear regression fitting curve is shown ($R = 0.97$).

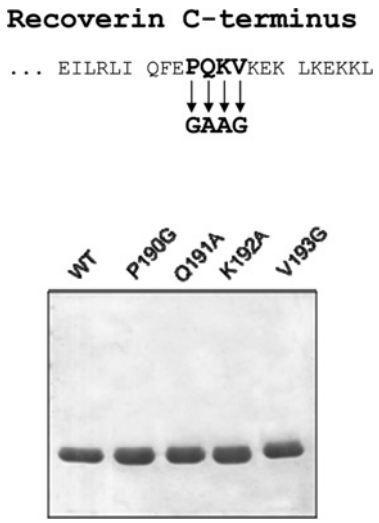

Figure 5 SDS/PAGE analysis of purified C-terminal point mutants of recoverin

The C-terminal sequence of recoverin is shown above the gel with amino acid substitutions highlighted in bold.

C-terminus might interact directly with residues from the N-terminal amphipathic helix of RK, presumably with Phe^3. We constructed the corresponding point mutants, expressed them heterologously in *E. coli* and purified them to apparent homogeneity (Figure 5). The recoverin point mutations did not affect the thermal stability of the protein, neither in the apo nor in the Ca^{2+}-bound form (Table 3); $^{45}Ca^{2+}$ binding was only slightly different for the Rc^{P190G} mutant (K_d was 28.5 μM in comparison with 19.2 μM for WT) and the co-operativity was lower for the Rc^{Q191A} mutant. All recoverin point mutants bound to membranes in the presence of Ca^{2+} similar to WT with EC_{50} values that were centred on 4.5 μM. Thus neither Ca^{2+}-binding properties nor Ca^{2+}-dependent membrane association of recoverin were affected by the introduced mutations. Interaction of recoverin point mutants with N-RK was studied in the same manner as the interaction with the truncated mutants (Figures 3 and 6). All mutants with the exception of Rc^{Q191A} had a lower affinity for N-RK as it became visible by pull-down experiments (Figure 6A) and SPR measurements (Figure 6B). However, the increase in the apparent K_d values was not so pronounced as what we observed with the truncated mutants (Table 3). The highest K_d of 34.1 μM was measured with the Rc^{K192A} mutant (Figure 6B), indicating that the lysine residue at this position is of critical importance for the interaction with RK. Point mutations also diminished the inhibitory effect of WT recoverin on RK, and the effect was largest with the mutants Rc^{K192A} and Rc^{V193G} (Figure 6C, inset), both also displayed the lowest apparent affinity for N-RK among all point mutants tested (Table 3). The mutant Rc^{Q191A} was slightly anomalous in this aspect as it had a reduced ability to inhibit RK, although its affinity for RK was as that of WT recoverin.

We also tested the effect of replacing phenylalanine at position 3 in N-RK. This residue is situated in close proximity to the C-terminal α-helix of recoverin in the model of the recoverin–N-RK complex, and therefore might have a crucial role in the interaction process. We mutated this residue to alanine and examined effects of this substitution on the apparent affinity for recoverin. Employing SPR spectroscopy in a series of recoverin titration experiments we observed that the binding amplitudes of WT recoverin interacting with N-RK^{F3A} were sufficiently diminished (Figure 6B). This is consistent with our suggestion that phenylalanine at position 3 is of primary importance for the recoverin C-terminus interaction with N-RK. The effect was similar to the one we observed for the binding of N-RK to the mutant Rc$^{2–188}$ [the C-terminal α-helix completely deleted by truncation (Figure 3C)], which further supports a crucial role of Phe^3.

DISCUSSION

The turn off of a photoreceptor light response depends critically on the timely phosphorylation of rhodopsin by RK [31]. This step is under Ca^{2+}-dependent control of the NCS protein recoverin operating in a ternary complex [8,9]. Since the Ca^{2+}-dependent regulation of RK activity is of critical importance for the sensitivity regulation of a photoreceptor cell [32], we focused in the present study on the structural basis of this regulatory step. The C-terminus of recoverin has been described in a previous publication as an internal modulator of Ca^{2+} sensitivity [11]. In the present study we extend this work by showing that the C-terminus of recoverin (Phe^{188}–Leu^{202}) not only influences the binding of Ca^{2+}, but also is critical for the affinity of recoverin binding to RK (for a summary of these data see Table 2). Using this approach we discovered a novel interaction site at the recoverin–RK protein–protein interface.

Since our conclusions are based on experiments employing truncated recoverin forms, it is important to verify that the decrease in affinity for Ca^{2+} and N-RK was not caused by defective

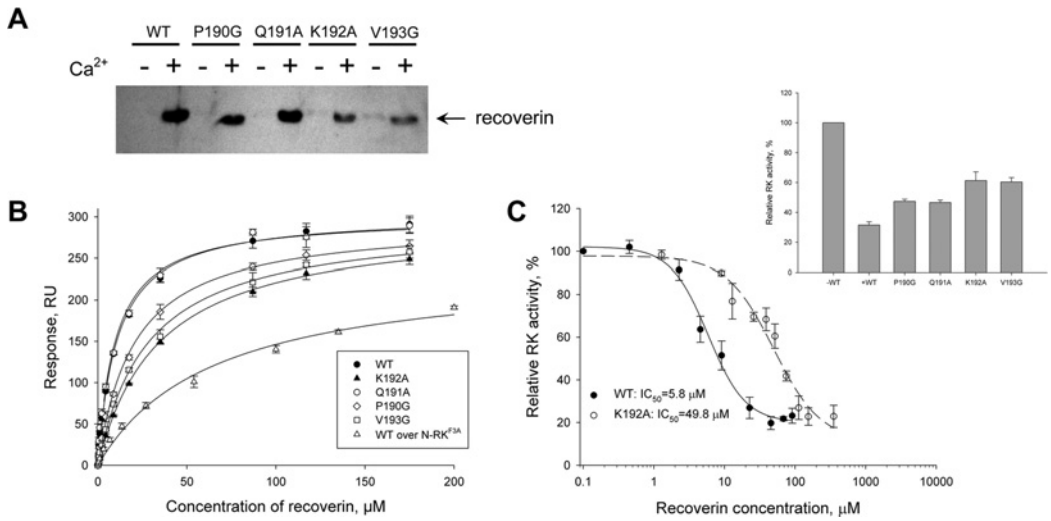

Figure 6 Effect of single amino acid substitutions in the C-terminus of recoverin on its interaction with N-RK

(**A**) Pull-down assay with recoverin point mutants after binding to N-RK immobilized on glutathione–Sepharose. The conditions were the same as applied to truncated mutants (Figure 3A). Recoverin bound on N-RK was visualized by anti-recoverin antibodies. (**B**) Effect of single amino acid substitution in N-RK and in the C-terminus of recoverin on the binding affinity measured by SPR spectroscopy. Binding of recoverin point mutants was recorded at different concentrations of recoverin and SPR amplitudes at equilibrium were determined, normalized and shown as a function of recoverin concentration, which was varied from 0.1 to 175 μM. The same protocol was used for recordings with WT recoverin and the N-RK^{F3A} mutant, which resulted in an apparent K_d of 65.2 $\pm$ 6.7 μM (S.D.). (**C**) Inhibition of RK by WT and Rc^{K192A}. RK activity was measured using an *in vitro* phosphorylation assay in the presence of 200 μM free Ca^{2+}. Phosphorylation of rhodopsin in the presence of other point mutants of recoverin is shown in the inset and was measured at 38 μM recoverin.

Table 3 The effect of single amino acid substitution in the C-terminal of recoverin on the thermal stability of the protein, its Ca^{2+}- binding parameters, Ca^{2+}-dependent interaction with ROS membranes and the affinity for N-RK

$T_{1/2}$, mid-transition temperature.

Recoverin form	Thermal denaturation*		Binding of Ca^{2+}†		Binding to membranes‡		Affinity for N-RK§
	$T_{1/2}$ (°C): apo form	$T_{1/2}$ (°C): Ca^{2+}-bound form	K_d (μM)	Hill coefficient	EC_{50}, $[Ca^{2+}]_f$ (μM)	Hill coefficient	K_d (μM)
WT	65.1	79.8	19.2 $\pm$ 0.4	1.78	3.5 $\pm$ 0.2	2.0	10.7 $\pm$ 0.6
P190G	64.8	78.1	28.5 $\pm$ 1.1	1.45	4.5 $\pm$ 0.3	2.0	20.5 $\pm$ 1.2
Q191A	65.5	80.8	19.0 $\pm$ 0.4	1.39	5.8 $\pm$ 0.3	1.5	9.8 $\pm$ 0.7
K192A	66.1	81.4	21.9 $\pm$ 0.6	1.48	4.9 $\pm$ 0.3	2.3	34.1 $\pm$ 1.5
V193G	66.5	80.7	20.3 $\pm$ 0.8	1.59	4.2 $\pm$ 0.3	2.5	28.0 $\pm$ 1.6

*Thermal denaturation of recoverin forms was monitored by tryptophan fluorescence of the protein.

†Ca^{2+}-binding parameters were measured by $^{45}Ca^{2+}$-binding assay.

‡Binding of recoverin forms to ROS membranes were measured at different $[Ca^{2+}]_f$ using an equilibrium centrifugation assay.

§The affinity of recoverin forms to N-RK were studied using SPR spectroscopy. The binding sensorgrams were recorded upon consecutive injections of Ca^{2+}-loaded recoverin forms at increasing concentrations over a sensorchip surface coated with N-RK via an anti-GST antibody. The equilibrium binding constants (K_D) are based on half-maximal concentration of recoverin required for saturation (Figure 6B).

folding of recoverin mutants. Using thermal denaturation studies we showed that mutants Rc$^{2–196}$, Rc$^{2–192}$, Rc$^{2–190}$ and Rc$^{2–188}$ have the same structural stability as recoverin WT and in the same time they exhibited lower affinity towards N-RK binding (Table 2 and Figure 2A). However, further shortening of the recoverin C-terminus in mutants Rc$^{2–187}$, Rc$^{2–186}$ and Rc$^{2–184}$ revealed progressive destabilization of the recoverin tertiary structure. In our previous publication [11], we indicated critical residues Phe^{188} and Ile^{186} forming a link to the cluster of non-polar residues in the central part of the recoverin structure (EF-hands 3 and 4). These contacts contribute to the hydrophobic core of recoverin, and disturbing them in the mutants Rc$^{2–187}$, Rc$^{2–186}$ and Rc$^{2–184}$ destabilized the protein structure. Of lesser importance for these intramolecular interactions are residues following Phe^{188} at the C-terminus. However, the results of the present study indicate their important role for the intermolecular interaction of recoverin with RK.

The Ca^{2+}-induced conformational change in recoverin exposes a number of non-polar amino acids in the N-terminal region that are involved in the interaction of recoverin to RK, and a recent NMR study using a 25 amino acid peptide of the N-terminus of RK (RK$^{1–25}$) revealed that the RK peptide adopts an amphipathic helix fitting into the hydrophobic groove of recoverin [9,10]. Other members of the NCS protein family such as KChIP1 [26], GCAP2 [27] and yeast frequenin [33] also harbour hydrophobic grooves considered to be important for target interaction. Previous studies have also shown an involvement of the C-terminal part of NCS proteins in their binding to target [26,34–37]. Using SPR measurements and pull-down assays, we found that the same is true for the C-terminus of recoverin. Importantly, the effects of reduced affinity of recoverin C-terminal mutants to RK revealed are not the result of an alteration in the Ca^{2+} sensitivity of recoverin, since all of the experiments were performed at saturating Ca^{2+} concentrations when recoverin is already in the

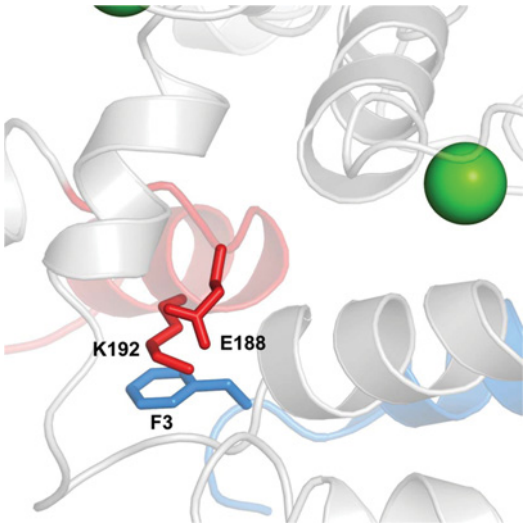

Figure 7 Structural details of the N-RK–recoverin interaction highlighting the contact region involving the C-terminus of recoverin and RK$^{1\text{-}25}$

The residues suggested to be most important for the interaction are shown in sticks and labelled (blue Phe^{3} from RK and red Lys^{192} and Gln^{188} from recoverin).

Ca^{2+}-loaded state. Moreover, the recoverin point mutants studied have almost the same Ca^{2+} sensitivity as WT recoverin, but lower affinity for RK (Table 3).

The C-terminal α-helix of recoverin following the kink caused by Pro^{190} provides additional contacts to the RK peptide, as it is apparent from the visual inspection of the three-dimensional model of the recoverin–N-RK complex (Figure 4A). Furthermore, our modelling approach highlighted the possible involvement of four amino acids in the C-terminus (Pro^{190}–Val^{193}) (Figure 4A). Thus the N-terminal peptide of RK is retained in the complex not only by the hydrophobic groove of recoverin, but also by additional contacts within the C-terminus of recoverin that provide more tight interaction and proper positioning of the target peptide. Our rigid-body docking simulations revealed a sufficient decrease in kinase peptide binding energy upon step-wise truncation of recoverin C-terminal α-helix, which is in agreement with the K_d values on interaction of truncated recoverin forms to immobilized N-RK (Table 2 and Figure 4B).

The major effect observed experimentally with the point mutant Rc^{K192A} [3.2-fold lower affinity for N-RK (Table 3) and 8.6-fold less inhibitory efficiency (Figure 6C)] was also in agreement with structural analysis. Lys^{192} was predicted to form a cation–π interaction pair with the aromatic ring of Phe^{3} in N-RK following the minor rearrangement of both residue side groups for optimal contact (Figure 7). Figure 7 also highlights a salt bridge between Lys^{192} and Glu^{188} at the recoverin C-terminus. Such an electrostatic interaction is expected to stabilize the orientation of the subsequent α-helix, hence providing an optimal orientation of the whole helix and creating the conditions for tight binding of Phe^{3} through the cation–π interaction with Lys^{192}. We confirmed these structural interpretations by measuring the affinity of the corresponding point mutant N-RK^{F3A} for recoverin that resulted in a similar affinity, like we obtained for the truncated recoverin mutant Rc$^{2-188}$ and N-RK (Figure 6B). These results were also broadly consistent with previous work using several point mutants of a 15 amino acid peptide of N-RK [10]. For example, mutations of Phe^{3} and Leu^{6} cause a complete loss of recoverin binding in pull-down assays. Whereas the residue Leu^{6} forms the tight contact with residues of the hydrophobic groove in recoverin [9], the interaction partner for residue Phe^{3}, until the start of the present study, was unknown.

Site-specific mutations of the three other amino acid residues in the recoverin C-terminus (P190G, Q191A and V193G) revealed a 2–3-fold lower N-RK affinity for Rc^{P190G} and Rc^{V193G}, but no effect of mutation at Gln^{191}. Since proline is known to determine the direction of an α-helix when located at the beginning of it, it probably helps to maintain the correct orientation of the recoverin C-terminus to the N-RK residues. A mutation to glycine would allow more flexibility and thus a less optimal interface. Val^{193} is faced almost at the opposite site of the helix with respect to the RK peptide and therefore is very likely to not be located in the interface region. Glycine is known as an helix breaker and its placement in position 193 instead of valine could therefore perturb the secondary structure of the whole C-terminal α-helix, thereby decreasing the protein affinity for N-RK (Table 3).

Taken together, the results of the present study demonstrate an important role of C-terminal segment of recoverin for RK targeting. We found that the binding surface for RK is not limited by the hydrophobic groove within the N-terminal lobe of recoverin, but also includes the last α-helix of C-terminal lobe. Involvement of distinct regions including the C-terminus in target binding or recognition is not uncommon among NCS proteins as this has been described for KChIP1 [26] and GCAP1 [34–37]. It will be of interest to see whether the cation–π interactions that have been observed in ligand–receptor interactions, as well as in enzymatic catalysis [38], also contribute significantly to NCS protein-related target recognition.

AUTHOR CONTRIBUTION

Evgeni Zernii and Konstantin Komolov were involved in experimental design, data collection, treatment and analysis, manuscript preparation and the overall design of the study. Sergei Permyakov was involved in experimental design, data treatment and analysis, and manuscript preparation. Tatiana Kolpakova was involved in data collection, and data treatment and analysis. Daniele Dell'Orco was involved in modelling and docking simulations, and manuscript preparation. Annika Poetzsch, Ekaterina Knyazeva, Ilya Grigoriev and Ekaterina Knyazeva were involved in data collection, and data treatment and analysis. Eugene A. Permyakov was involved in experimental design and manuscript preparation. Ivan I. Senin was involved in experimental design, data collection, treatment and analysis, and the overall design of the study. Pavel P. Philippov was involved in data treatment and analysis, and manuscript preparation. Karl-Wilhelm Koch was involved in the experimental design, data treatment and analysis, manuscript preparation and the overall design of the study.

ACKNOWLEDGEMENTS

We thank Dmitry V. Zinchenko for the HPLC analysis of recoverin samples.

FUNDING

This work was supported by the Russian Foundation for Basic Research [grant numbers 09-04-01778-a (to I.I.S.), 09-04-00666-a (to E.Yu.Z.)]; the President of Russia [grant number MD-4423.2010.4 (to I.I.S.)]; in part by the Russian Foundation for Basic Research [grant number 09-04-00395 (to P.P.Ph.)]; the Program of the Russian Academy of Sciences "Molecular and Cellular Biology" (to P.E.A); the Deutsche Forschungsgemeinschaft (DFG) [grant numbers KO948/7-1, KO948/7-2 (to K.W.K.)]. The use of the computer cluster for simulations was supported by the EC integrated Project DIRAC, in the 6th FWP under IST-02778. D.D.O. is the recipient of an Alexander von Humboldt Fellowship.

REFERENCES

1 Berridge, M. J., Lipp, P. and Bootman, M. D. (2000) The versatility and universality of calcium signalling. Nat. Rev. Mol. Cell Biol. **1**, 11–21

2 Ikura, M. and Ames, J. B. (2006) Genetic polymorphism and protein conformational plasticity in the calmodulin superfamily: two ways to promote multifunctionality. Proc. Natl. Acad. Sci. U.S.A. **103**, 1159–1164

3 Rizo, J. and Sudhof, T. C. (1998) C2-domains, structure and function of a universal Ca^{2+}-binding domain. J. Biol. Chem. **273**, 15879–15882

4 Lewit-Bentley, A. and Rety, S. (2000) EF-hand calcium-binding proteins. Curr. Opin. Struct. Biol. **10**, 637–643

5 Burgoyne, R. D. (2007) Neuronal calcium sensor proteins: generating diversity in neuronal Ca^{2+} signalling. Nat. Rev. Neurosci. **8**, 182–193

6 Philippov, P. P. and Koch, K. -W. (eds) (2006) Neuronal Calcium Sensor Proteins, Nova Publishers, Hauppauge

7 Burgoyne, R. D. and Weiss, J. L. (2001) The neuronal calcium sensor family of Ca^{2+}-binding proteins. Biochem. J. **353**, 1–12

8 Komolov, K. E., Senin, I. I., Kovaleva, N. A., Christoph, M. P., Churumova, V. A., Grigoriev, I. I., Akhtar, M., Philippov, P. P. and Koch, K. W. (2009) Mechanism of rhodopsin kinase regulation by recoverin. J. Neurochem. **110**, 72–79

9 Ames, J. B., Levay, K., Wingard, J. N., Lusin, J. D. and Slepak, V. Z. (2006) Structural basis for calcium-induced inhibition of rhodopsin kinase by recoverin. J. Biol. Chem. **281**, 37237–37245

10 Higgins, M. K., Oprian, D. D. and Schertler, G. F. (2006) Recoverin binds exclusively to an amphipathic peptide at the N terminus of rhodopsin kinase, inhibiting rhodopsin phosphorylation without affecting catalytic activity of the kinase. J. Biol. Chem. **281**, 19426–19432

11 Weiergräber, O. H., Senin, I. I., Zernii, E. Y., Churumova, V. A., Kovaleva, N. A., Nazipova, A. A., Permyakov, S. E., Permyakov, E. A., Philippov, P. P., Granzin, J. and Koch, K. W. (2006) Tuning of a neuronal calcium sensor. J. Biol. Chem. **281**, 37594–37602, J. Biol. Chem. **281**, 19426–19432

12 Senin, I. I., Fischer, T., Komolov, K. E., Zinchenko, D. V., Philippov, P. P. and Koch, K. W. (2002) Ca^{2+}-myristoyl switch in the neuronal calcium sensor recoverin requires different functions of Ca^{2+}-binding sites. J. Biol. Chem. **277**, 50365–50372

13 Johnson, Jr, W. C., Palczewski, K., Gorczyca, W. A., Riazance-Lawrence, J. H., Witkowska, D. and Polans, A. S. (1997) Calcium binding to recoverin: implications for secondary structure and membrane association. Biochim. Biophys. Acta **1342**, 164–174

14 Weiergraber, O. H., Senin, I. I., Philippov, P. P., Granzin, J. and Koch, K. W. (2003) Impact of N-terminal myristoylation on the Ca^{2+}-dependent conformational transition in recoverin. J. Biol. Chem. **278**, 22972–22979

15 Permyakov, S. E., Khokhlova, T. I., Uversky, V. N. and Permyakov, E. A. (2010) Analysis of Ca^{2+}/Mg^{2+} selectivity in α-lactalbumin and Ca^{2+}-binding lysozyme reveals a distinct Mg^{2+}-specific site in lysozyme. Proteins **78**, 2609–2624

16 Zozulya, S. and Stryer, L. (1992) Calcium-myristoyl protein switch. Proc. Natl. Acad. Sci. U.S.A. **89**, 11569–11573

17 Komolov, K. E., Zinchenko, D. V., Churumova, V. A., Vaganova, S. A., Weiergraber, O. H., Senin, I. I., Philippov, P. P. and Koch, K. W. (2005) One of the Ca^{2+} binding sites of recoverin exclusively controls interaction with rhodopsin kinase. Biol. Chem. **386**, 285–289

18 Lambrecht, H. G. and Koch, K. W. (1992) Recoverin, a novel calcium-binding protein from vertebrate photoreceptors. Biochim. Biophys. Acta **1160**, 63–66

19 Lange, C. and Koch, K. W. (1997) Calcium-dependent binding of recoverin to membranes monitored by surface plasmon resonance spectroscopy in real time. Biochemistry **36**, 12019–12026

20 Koch, K. W. (2000) Identification and characterization of calmodulin binding sites in cGMP-gated channel using surface plasmon resonance spectroscopy. Methods Enzymol. **315**, 785–797

21 Komolov, K. E., Senin, I. I., Philippov, P. P. and Koch, K. W. (2006) Surface plasmon resonance study of g protein/receptor coupling in a lipid bilayer-free system. Anal. Chem. **78**, 1228–1234

22 Dell'Orco, D. (2009) Fast predictions of thermodynamics and kinetics of protein–protein recognition from structures: from molecular design to systems biology. Mol. Biosyst. **5**, 323–334

23 Dell'Orco, D., Seeber, M., De Benedetti, P. G. and Fanelli, F. (2005) Probing fragment complementation by rigid-body docking: *in silico* reconstitution of calbindin D9k. J. Chem. Inf. Model. **45**, 1429–1438

24 Chen, R. and Weng, Z. (2003) A novel shape complementarity scoring function for protein–protein docking. Proteins **51**, 397–408

25 Dell'Orco, D., De Benedetti, P. G. and Fanelli, F. (2007) *In silico* screening of mutational effects on enzyme-protein inhibitor affinity: a docking-based approach. BMC Struct. Biol. **7**, 37

26 Zhou, W., Qian, Y., Kunjilwar, K., Pfaffinger, P. J. and Choe, S. (2004) Structural insights into the functional interaction of KChIP1 with Shal-type K^+ channels. Neuron **41**, 573–586

27 Ermilov, A. N., Olshevskaya, E. V. and Dizhoor, A. M. (2001) Instead of binding calcium, one of the EF-hand structures in guanylyl cyclase activating protein-2 is required for targeting photoreceptor guanylyl cyclase. J. Biol. Chem. **276**, 48143–48148

28 Tachibanaki, S., Nanda, K., Sasaki, K., Ozaki, K. and Kawamura, S. (2000) Amino acid residues of S-modulin responsible for interaction with rhodopsin kinase. J. Biol. Chem. **275**, 3313–3319

29 Dell'Orco, D., Casciari, D. and Fanelli, F. (2008) Quaternary structure predictions and estimation of mutational effects on the free energy of dimerization of the OMPLA protein. J. Struct. Biol. **163**, 155–162

30 Dell'Orco, D., De Benedetti, P. G. and Fanelli, F. (2007) *In silico* screening of mutational effects on transmembrane helix dimerization: insights from rigid-body docking and molecular dynamics simulations. J. Phys. Chem. B **111**, 9114–9124

31 Mendez, A., Burns, M. E., Roca, A., Lem, J., Wu, L. W., Simon, M. I., Baylor, D. A. and Chen, J. (2000) Rapid and reproducible deactivation of rhodopsin requires multiple phosphorylation sites. Neuron **28**, 153–164

32 Chen, C. -K., Woodruff, M. L., Chen, F. S., Chen, D. and Fain, G. F. (2010) Background light produces a recoverin-dependent modulation of activated-rhodopsin lifetime in mouse rods. J. Neurosci. **30**, 1213–1220

33 Strahl, T., Huttner, I. G., Lusin, J. D., Osawa, M., King, D., Thorner, J. and Ames, J. B. (2007) Structural insights into activation of phosphatidylinositol 4-kinase (Pik1) by yeast frequenin (Frq1). J. Biol. Chem. **282**, 30949–30959

34 Krylov, D. M., Niemi, G. A., Dizhoor, A. M. and Hurley, J. B. (1999) Mapping sites in guanylyl cyclase activating protein-1 required for regulation of photoreceptor membrane guanylyl cyclases. J. Biol. Chem. **274**, 10833–10839

35 Schrem, A., Lange, C., Beyermann, M. and Koch, K. W. (1999) Identification of a domain in guanylyl cyclase-activating protein 1 that interacts with a complex of guanylyl cyclase and tubulin in photoreceptors. J. Biol. Chem. **274**, 6244–6249

36 Li, N., Sokal, I., Bronson, J. D., Palczewski, K. and Baehr, W. (2001) Identification of functional regions of guanylate cyclase-activating protein 1 (GCAP1) using GCAP1/GCIP chimeras. Biol. Chem. **382**, 1179–1188

37 Hwang, J. Y., Schlesinger, R. and Koch, K. W. (2004) Irregular dimerization of guanylate cyclase-activating protein 1 mutants causes loss of target activation. Eur. J. Biochem. **271**, 3785–3793

38 Zacharias, N. and Dougherty, D. A. (2002) Cation–pi interactions in ligand recognition and catalysis. Trends Pharmacol. Sci. **23**, 281–287

Received 4 January 2011/4 February 2011; accepted 8 February 2011
Published as BJ Immediate Publication 8 February 2011, doi:10.1042/BJ20110013